

## Photochemical Reaction Pathways of Carbon Tetrabromide in Solution Probed by Picosecond X-ray Diffraction

Qingyu Kong,<sup>†</sup> Michael Wulff,<sup>†</sup> Jae Hyuk Lee,<sup>‡</sup> Savo Bratos,<sup>§</sup> and Hyotcherl Ihee<sup>\*‡</sup>

Contribution from the European Synchrotron Radiation Facility, Grenoble Cedex 38043, BP 220, France, National Creative Research Initiative Center for Time-Resolved Diffraction, Department of Chemistry and School of Molecular Science (BK21), Korea Advanced Institute of Science and Technology (KAIST), Daejeon, 305-701, Republic of Korea, and Laboratoire de Physique, Théorique des Liquides, Université Pierre et Marie Curie, Case Courrier 121, 4 Place Jussieu, Paris Cedex 75252, France

Received June 1, 2007; E-mail: hyotcherl.ihee@kaist.ac.kr

**Abstract:** We report a liquid-phase time-resolved X-ray diffraction study that resolves the molecular structures of the short-lived intermediates formed in the photodissociation of tetrabromomethane in methanol. Time-resolved X-ray diffraction can detect all chemical species simultaneously, and the diffraction signal from each chemical species can be quantitatively calculated from molecular structures and compared with experimental data with high accuracy and precision. The photochemistry of carbon tetrahalides has long been explored to describe their reactions in the natural environment due to its relevance to ozone depletion. Excited with an ultraviolet optical pulse, the complicated photodissociation dynamics of  $\text{CBr}_4$  was followed in a wide temporal range from picoseconds up to microseconds and associated rate coefficients were determined by analyzing time-resolved diffraction patterns accumulated from 100 ps X-ray pulses. The homolytic cleavage of one C–Br bond in the parent  $\text{CBr}_4$  molecule yields the  $\text{CBr}_3$  and Br radicals, which escape from the solvent cage and combine nongeminately to form  $\text{C}_2\text{Br}_6$  and  $\text{Br}_2$ , respectively.  $\text{C}_2\text{Br}_6$  eventually decays to give  $\text{C}_2\text{Br}_4$  and  $\text{Br}_2$  as final stable products. Our diffraction data at the current signal-to-noise ratio could not provide any evidence for the geminate recombination of the  $\text{CBr}_3$  and Br radicals to form the  $\text{Br}_2\text{CBr}$ –Br isomer or the solvated ion pair, implying that their formation is a minor channel compared with those observed clearly by time-resolved diffraction in this work.

### Introduction

Accurate determination of molecular structures has been one of the most challenging and enduring subjects in chemistry.<sup>1–5</sup> Hard X-ray photons with a wavelength around 1 Å interact not only with outer shell electrons but also with core electrons that directly indicate molecular geometry. X-ray diffraction is thus a powerful method in determining molecular structures from both crystal and liquid phases.<sup>6–9</sup> Time-resolved X-ray diffraction that combines the spatial and temporal measurements can

resolve the molecular structures of short-lived intermediates and free radicals in a chemical reaction, and a number of important results have been provided by this technique.<sup>10–16</sup> Time-resolved electron diffraction is another powerful method to determine the structures of short-lived intermediates.<sup>17,18</sup>

Carbon tetrahalides are found in the natural environment and are important sources of reactive halogens that have been linked to ozone depletion in both the troposphere and the stratosphere.<sup>19–22</sup> Their photochemistry in the gas and condensed phases has

<sup>†</sup> European Synchrotron Radiation Facility.

<sup>‡</sup> Korea Advanced Institute of Science and Technology (KAIST).

<sup>§</sup> Université Pierre et Marie Curie.

(1) Pratt, D. W. *Annu. Rev. Phys. Chem.* **1998**, *49*, 481.

(2) Bak, K. L.; Gauss, J.; Jørgensen, P.; Olsen, J.; Helgaker, T.; Stanton, J. F. *J. Chem. Phys.* **2001**, *114*, 6548.

(3) Johnson, M. R.; Jones, N. H.; Geis, A.; Horsewill, A. J.; Trommsdorff, H. P. *J. Chem. Phys.* **2002**, *116*, 5694.

(4) Qiu, W.; Wang, L.; Lu, W.; Boechler, A.; Sanders, D. A. R.; Zhong, D. *Proc. Natl. Acad. Sci. U.S.A.* **2007**, *104*, 5366.

(5) Qiu, W.; Zhang, L.; Okobiah, O.; Yang, Y.; Wang, L.; Zhong, D.; Zewail, A. H. *J. Phys. Chem. B* **2006**, *110*, 10540.

(6) Glandorf, L. N.; Scheer, M.; Samuels, D. A.; Mulhisen, A. M.; Grant, E. R.; Yang, X. M.; Bierbaum, V. M.; Leone, S. R. *Phys. Rev. Lett.* **2001**, *87*, 193002.

(7) Glandorf, L. N.; Scheer, M.; Samuels, D. A.; Bierbaum, V. M.; Leone, S. R. *J. Chem. Phys.* **2002**, *117*, 6108.

(8) Musgrave, K. B.; Laplaza, C. E.; Holm, R. H.; Hedman, B.; Hodgson, K. O. *J. Amer. Chem. Soc.* **2002**, *124*, 3083.

(9) Miao, J.; Hodgson, K. O.; Sayre, D. *Proc. Natl. Acad. Sci. U.S.A.* **2001**, *98*, 6641.

(10) Rousse, A.; Rischel, C.; Fourmaux, S.; Uschmann, I.; Sebban, S.; Grillon, G.; Balcou, P.; Foster, E.; Geindre, J. P.; Audebert, P.; Gauthier, J. C.; Hulin, D. *Nature* **2001**, *410*, 65.

(11) Adachi, S.; Park, S. Y.; Tame, J. R. H.; Shiro, Y.; Shibayama, N. *Proc. Natl. Acad. Sci. U.S.A.* **2003**, *100*, 7039.

(12) Bratos, S.; Mirloup, F.; Vuilleumier, R.; Wulff, M.; Plech, A. *Chem. Phys.* **2004**, *304*, 245.

(13) Plech, A.; Wulff, M.; Bratos, S.; Mirloup, F.; Vuilleumier, R.; Schotte, F.; Anfinrud, P. A. *Phys. Rev. Lett.* **2004**, *92*, 125505.

(14) Ihee, H.; Lorenc, M.; Kim, T. K.; Kong, Q. Y.; Cammarata, M.; Lee, J. H.; Bratos, S.; Wulff, M. *Science* **2005**, *309*, 1223.

(15) Kim, T. K.; Lorenc, M.; Lee, J. H.; Lo Russo, M.; Kim, J.; Cammarata, M.; Kong, Q. Y.; Noel, S.; Plech, A.; Wulff, M.; Ihee, H. *Proc. Natl. Acad. Sci. U.S.A.* **2006**, *103*, 9410.

(16) Lee, J. H.; Kim, K. H.; Kim, T. K.; Lee, Y. H.; Ihee, H. *J. Chem. Phys.* **2006**, *125*, 174504.

(17) Nie, S.; Wang, X.; Park, H.; Clinite, R.; Cao, J. *Phys. Rev. Lett.* **2006**, *96*, 025901.

(18) Cao, J.; Hao, Z.; Park, H.; Tao, C.; Kau, D.; Blaszczyk, L. *Appl. Phys. Lett.* **2003**, *83*, 1044.

(19) Molina, M. J.; Rowland, F. S. *Nature* **1974**, *249*, 810.

(20) Molina, M. J.; Tso, T. L.; Molina, L. T.; Wang, F. C. Y. *Science* **1987**, *238*, 1253.

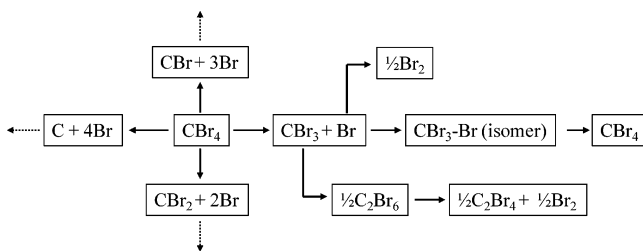


**Figure 1.** Candidate reaction pathways for CBr<sub>4</sub>. The photodissociation of CBr<sub>4</sub> unfolds the most complex photochemical reaction pathways ever studied with time-resolved X-ray diffraction since at least 10 candidate chemical species can be involved.

therefore become an area of active investigation.<sup>23–27</sup> Studies of the photodissociation of tetrabromomethane (CBr<sub>4</sub>) by time-resolved laser and X-ray absorption spectroscopy<sup>28–30</sup> have led to contradictory results. The picosecond Raman spectroscopic study of CBr<sub>4</sub> in cyclohexane showed that the Br<sub>2</sub>CBr–Br isomer with a lifetime of nanoseconds is formed after UV excitation.<sup>28</sup> By contrast, a recent time-resolved absorption spectroscopic study suggested that one photon excitation of CBr<sub>4</sub> at 266 nm in various nonpolar and polar solvents such as cyclohexane, dodecane, 1-octanol, 2-propanol, acetonitrile, and propylene carbonate results in the formation of a solvent-stabilized solvated ion pair (CBr<sub>3</sub><sup>+</sup>//Br<sup>−</sup>)<sub>solv</sub> whose decay time constants depend on the solvent and range from subnanoseconds to microseconds.<sup>29</sup> The ultrafast EXAFS study on CBr<sub>4</sub> in cyclohexane did not show any photodissociated intermediates.<sup>30</sup> These discrepancies suggested that it would be useful to check the photodissociation process of CBr<sub>4</sub> in solution by time-resolved X-ray diffraction. In this work, we chose methanol as the solvent because it is one of the common solvents and its diffraction intensity, which is an indispensable ingredient in the data analysis, was well characterized in our previous studies.<sup>12–15</sup> Methanol whose dielectric constant is about 33 should correlate well with other polar solvents such as acetonitrile (dielectric constant of 37) and 2-propanol (dielectric constant of 20).

The photodissociation of CBr<sub>4</sub> presents one of the most complex photochemical reaction pathways ever studied with time-resolved X-ray diffraction since at least 10 candidate chemical species can be involved (Figure 1). Compared to ultrafast optical spectroscopy, diffraction offers the important advantage that the scattered X-rays contain contributions from all chemical species in the volume probed by the X-ray beam, and a “global” detection of all intermediates can be obtained.<sup>12–15</sup> Our results provide a complete description of the photodissociation reaction of tetrabromomethane in solution and reveal the existence of new intermediates which had not been detected in the previous optical spectroscopic studies. This resolves the

**Table 1.** Directly and Nondirectly Bonded C–Br and Br–Br Internuclear Distances Calculated with DFT at B3LYP/6-311+G(3df) Level for the Chemical Species Considered in the Analysis<sup>a</sup>

species	C–Br/C···Br (Å)	Br–Br/Br···Br (Å)
CBr <sub>4</sub>	1.957	3.196
CBr <sub>3</sub>	1.885	3.221
CBr <sub>3</sub> <sup>+</sup>	1.819	3.150
CBr <sub>2</sub>	1.894	3.120
Br <sub>2</sub>	–	2.316
C <sub>2</sub> Br <sub>6</sub>	1.966, 2.920	3.183, 3.493, 4.725
C <sub>2</sub> Br <sub>4</sub>	1.892, 2.849	3.175, 3.395, 4.648
CBr <sub>3</sub> –Br isomer	1.844, 1.851, 4.628	2.849, 3.210, 3.161, 5.746
C <sub>2</sub> Br <sub>5</sub>	1.874, 2.866, 2.889	3.169, 3.170, 3.231, 3.388, 3.842, 4.639

<sup>a</sup> The SCIPCM model was used to include the solvent effect. A more detailed and complete structural information is provided in the Supporting Information.

inconsistencies in the literature and begins to address open questions concerning the photochemistry of carbon tetrahalides.

## Methods

**Experiments.** The experimental setup of ID09B at the ESRF has been described in detail in our previous studies.<sup>12–15</sup> Briefly, an ultraviolet optical pulse at 266 nm, which was stretched to around 2 ps with two fused silica prisms to avoid multiphoton absorption, is used to excite the CBr<sub>4</sub> molecules dissolved in methanol. The relaxation of the excited molecules was monitored with a delayed 100 ps (fwhm) X-ray pulse, selected with a synchronized mechanical chopper at a frequency of 998.6 Hz. A pink beam centered at 17.8 keV (0.70 Å) with a flux of  $5 \times 10^8$  photons per pulse produced from the U17 undulator was focused into a  $100 \times 60 \mu\text{m}^2$  spot on the sample by a toroidal mirror. CBr<sub>4</sub> (99%) and spectroscopic grade methanol (>99.8%) were purchased from Sigma-Aldrich and used without further purification. A diluted solution of 5 mM was prepared for the experiment, and a sapphire nozzle was used to cycle the solution, which produced a stable liquid sheet of  $\sim 300 \mu\text{m}$  thickness. The speed of the liquid is around 3 m/s. The scattered intensities from the sample were collected with an area detector (MarCCD, Mar USA, Evanston, IL). The CBr<sub>4</sub>/methanol solution was completely replaced with fresh solution every 2 h during the experiment since the photodissociation reaction generates irreversible products.

**DFT calculations.** Geometries of putative solutes in a methanol solvent model were optimized with density function theory (DFT) methods which are implemented in the Gaussian 03 program.<sup>31</sup> The Becke three-parameter hybrid functional with the Lee–Yang–Parr correlation corrections (B3LYP) level was used in the calculations.<sup>32,33</sup> The all-electron basis set 6-311+G(3df) for C and Br was used in the calculation. The self-consistent isodensity polarized continuum model (SCIPCM) of the self-consistent reaction field (SCRf) theory was used to describe the solvent effects.<sup>34</sup> Details about the DFT calculation can be found in our previous study.<sup>35</sup> Directly and nondirectly bonded C–Br and Br–Br internuclear distances of the calculated structures for the chemical species relevant to the analysis of the time-resolved diffraction data are listed in Table 1, and more detailed and complete structural information can be found in the Supporting Information.

**Molecular Dynamics (MD) Simulations.** The solute/solvent interactions (cage structure) were obtained by MD simulations using the

- (21) McElroy, C. T.; McLinden, C. A.; McConnell, J. C. *Nature* **1999**, *397*, 338.
- (22) Alicke, B.; Hebestreit, K.; Stutz, J.; Platt, U. *Nature* **1999**, *397*, 572.
- (23) Vogt, R.; Crutzen, P. J.; Sander, R. *Nature* **1996**, *383*, 327.
- (24) Oum, K. W.; Lakin, M. J.; DeHaan, D. O.; Brauers, T.; Finalyson-Pitts, B. J. *Science* **1998**, *279*, 74.
- (25) Knipping, E. M.; Lakin, M. J.; Foster, K. L.; Jungwirth, P.; Tobias, D. J.; Gerber, R. B.; Dabdub, D.; Finalyson-Pitts, B. J. *Science* **2000**, *288*, 301.
- (26) Finalyson-Pitts, B. J.; Hemminger, J. C. *J. Phys. Chem. A* **2000**, *104*, 11463.
- (27) Foster, K. L.; Plastring, R. A.; Bottenheim, J. W.; Shepson, P. B.; Finalyson-Pitts, B.; Spicer, J. C. W. *Science* **2001**, *291*, 471.
- (28) Zheng, X. M.; Fang, W. H.; Phillips, D. L. *J. Chem. Phys.* **2000**, *113*, 10934.
- (29) Zhang, H.; Dvornikov, A. S.; Rentzepis, P. M. *J. Phys. Chem. A* **2005**, *109*, 5984.
- (30) Oulianov, D. A.; Tomov, I. V.; Dvornikov, A. S.; Rentzepis, P. M. *Proc. Natl. Acad. Sci. U.S.A.* **2002**, *99*, 12556.

- (31) Frisch, M. J. et al. *Gaussian 03*, revision C.02; Gaussian, Inc.: Wallingford, CT, 2004.
- (32) Becke, A. D. *J. Chem. Phys.* **1993**, *98*, 5648.
- (33) Lee, C.; Yang, W.; Parr, R. G. *Phys. Rev. B* **1988**, *37*, 785.
- (34) Foresman, J. B.; Keith, T. A.; Wiberg, K. B.; Snoonian, J.; Frisch, M. J. *J. Phys. Chem.* **1996**, *100*, 16098.
- (35) Kong, Q. Y.; Wulff, M.; Bratos, S.; Vuilleumier, R.; Kim, J.; Ihee, H. *J. Phys. Chem. A* **2006**, *110*, 11178.

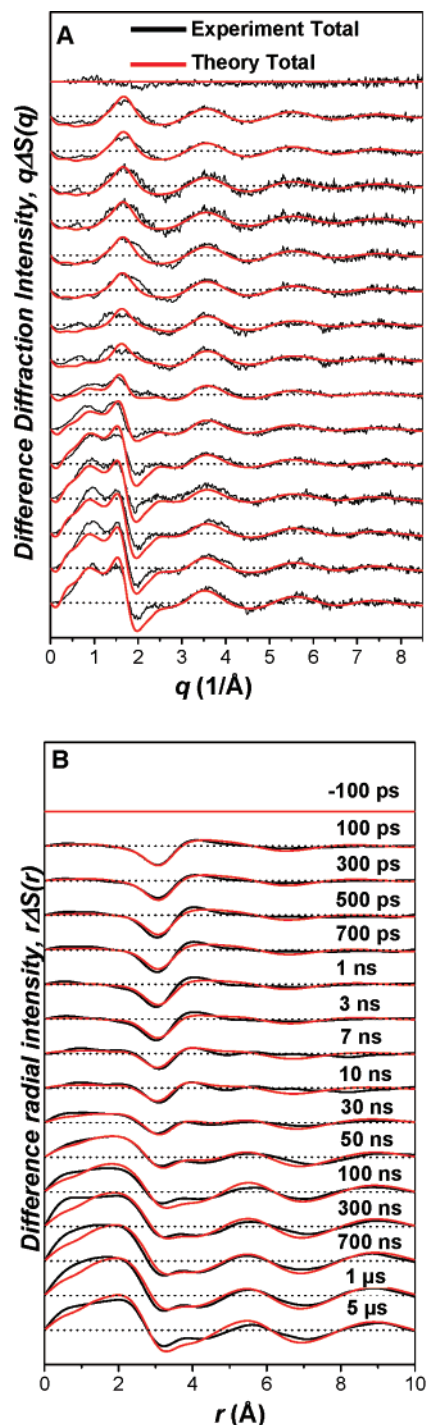


**Figure 2.** Time-resolved difference diffraction signal of  $\text{CBr}_4$  in methanol as a function of time delays. (A) Difference diffraction intensities,  $q\Delta S(q)$  at all time delays. Least-squares fits to a theoretical model are also shown (red curves). (B) Difference radial distribution curves,  $r\Delta S(r)$ , obtained by sine-Fourier transform of (A).

MOLDY program.<sup>36</sup> Detailed descriptions about our MD simulations and the cage structure extraction can be found in the reports of our previous studies.<sup>14,15</sup>

## Results and Discussion

### Difference Diffraction Curves and Radial Distribution Curves.

To follow the structural dynamics in the photodisso-

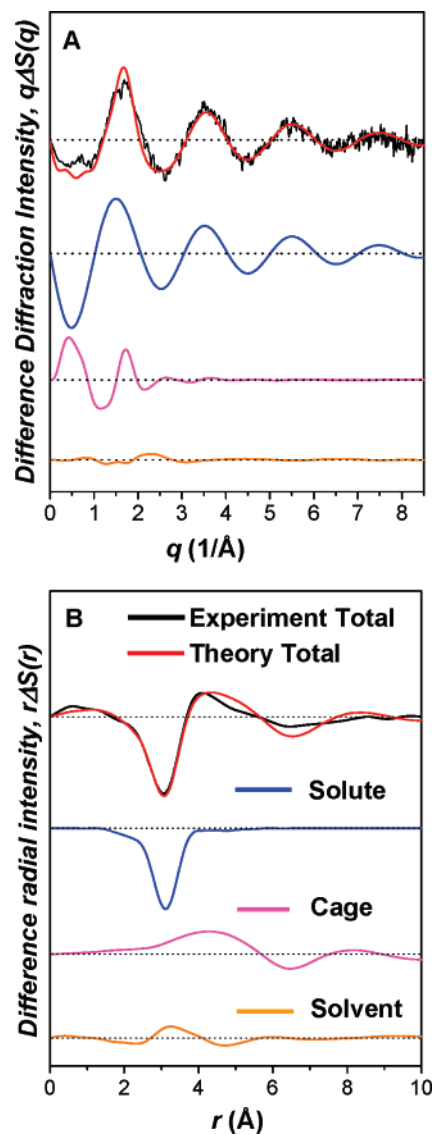


**Figure 3.** (A) Time-resolved structural reaction dynamics of  $\text{CBr}_4$  in methanol at 100 ps. The theoretical model (red curve) has three contributions: the transient solute (blue), solute/solvent interaction (magenta), and bulk solvent response due to thermal expansion and temperature change (orange). The solute signal is calculated from the Debye scattering of putative solutes, the solvent signal is deduced from impulsive heating of pure methanol excited with NIR optical pulse, and the solute/solvent interaction (cage) is calculated by MD. (B) Difference radial intensity  $r\Delta S(r)$  of  $\text{CBr}_4$  in methanol at 100 ps, through sine-Fourier transform of (A).

ciation process, a series of time-resolved X-ray scattering data were collected with time delays of  $-3$  ns,  $-100$  ps, 100 ps, 300 ps, 500 ps, 700 ps, 1 ns, 3 ns, 7 ns, 10 ns, 30 ns, 50 ns, 100 ns, 300 ns, 700 ns, 1  $\mu\text{s}$ , and 5  $\mu\text{s}$  relative to the UV-pulse. To extract the changes from the laser excitation only, difference images were generated by subtracting the images in the absence of the pump from the images in the presence of the optical pump. The data point at  $-3$  ns was used as a reference (absence of pump) in the subtraction, and another negative time delay at  $-100$  ps was used to check the validity of time zero. Detailed descriptions of the methods used to obtain difference images can be found in the reports of our previous studies.<sup>13–15</sup>

The difference diffraction intensities  $\Delta S(q)$ , obtained by radial integration of the difference CCD images, contain information on the structural changes of the probed solutions. To magnify the scattered intensities at high angles, the difference diffraction

(36) Refson, K. *Comp. Phys. Comm.* **2000**, *126*, 310.

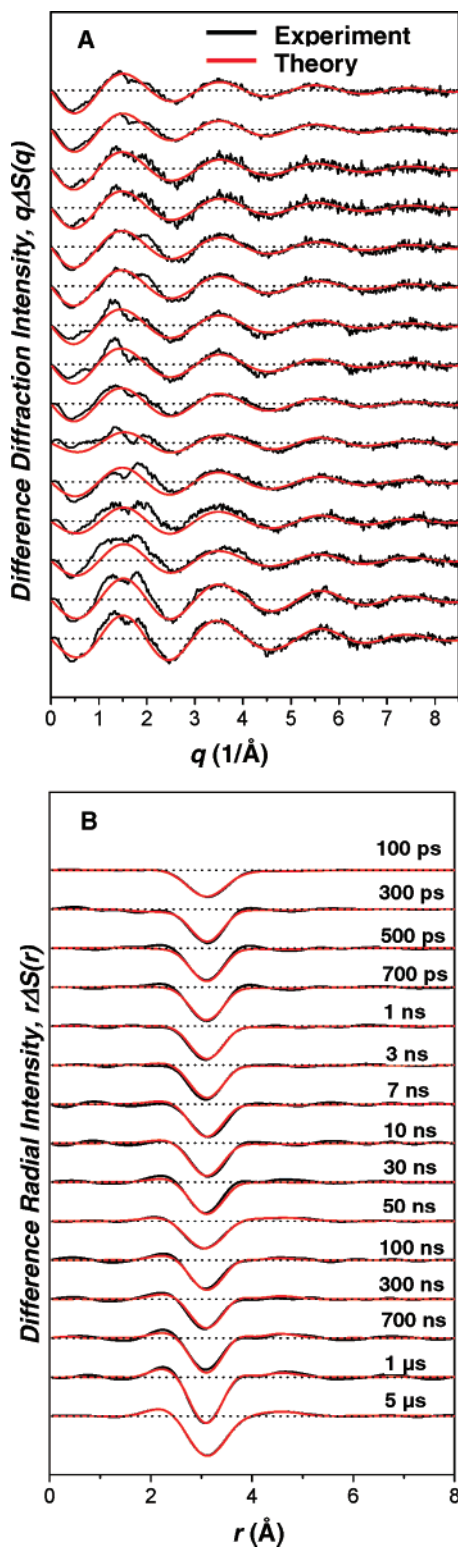


**Figure 4.** (A) Solute-only experimental (black) and theoretical (red) difference diffraction intensities  $q\Delta S(q)$ . (B) Solute-only difference radial intensity  $r\Delta S(r)$ , through sine-Fourier transform of A.

intensities were multiplied by  $q$ . Figure 2 shows the time-resolved difference diffraction signal of  $\text{CBr}_4$  in methanol as a function of time delays along with least-squared fits to a theoretical model. As shown in Figure 2, the difference signal at  $-100$  ps is zero, which confirms the accuracy of our time zero. At positive time delays, difference features appear and evolve with time.

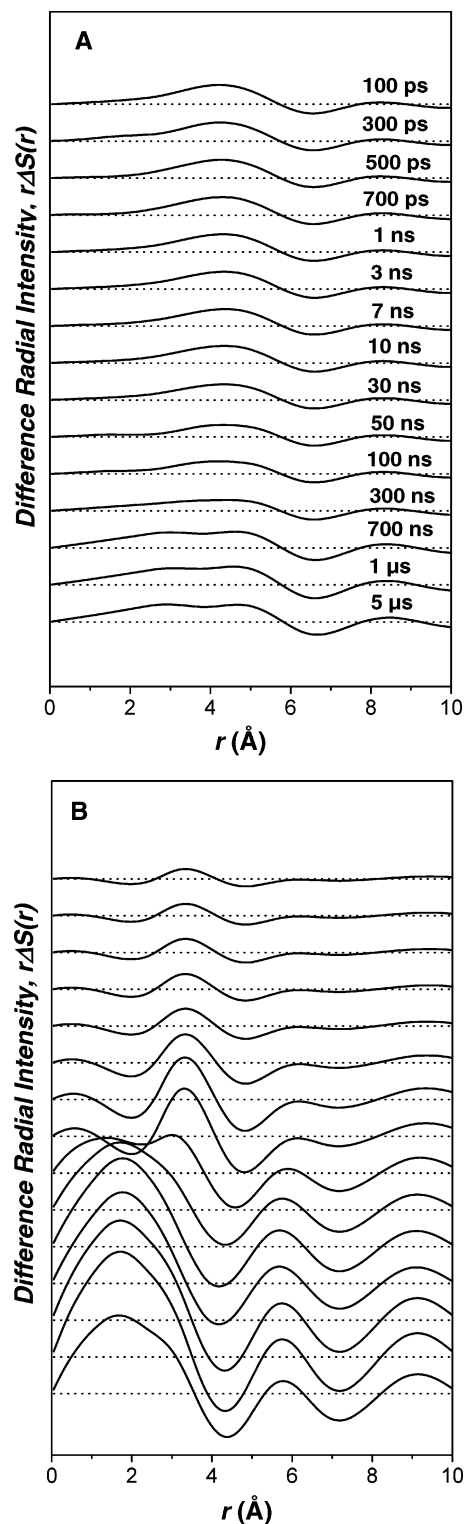


**Figure 5.** (A) Cage-only and (B) solvent-only difference radial intensity  $r\Delta S(r)$ .

Our previous studies<sup>14,15</sup> have confirmed that the total signal  $\Delta S(q)$  contains three contributions: the structural change of the solute, the change of the solvation cage caused by solute/solvent interactions, and the bulk solvent response to heating and thermal expansion. To explain the measured signal, a theoretical model including these three contributions was used to fit the experimental data. In the model, the structural change of the solute was calculated from the difference Debye scattering

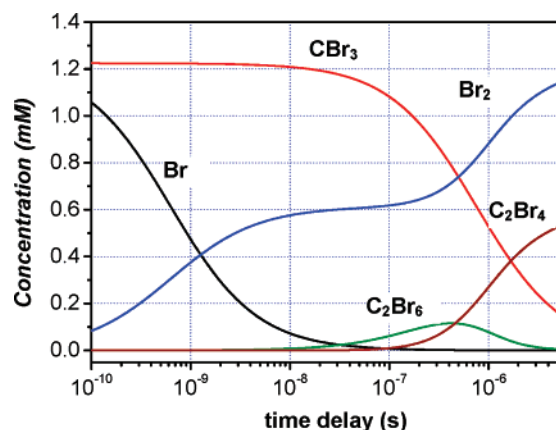


**Figure 6.** Population changes of various molecular species in the photodissociation reaction of  $\text{CBr}_4$  in methanol: the  $\text{CBr}_3$  (red) and  $\text{Br}$  (black) radicals, the intermediate  $\text{C}_2\text{Br}_6$  (olive), and the final products  $\text{Br}_2$  (blue) and  $\text{C}_2\text{Br}_4$  (wine) as a function of time delay.

between putative photoproducts and the parent molecule. The bulk solvent response was deduced from the measured impulsive heating of the pure solvent excited by near-infrared (NIR) laser photons,<sup>37</sup> and the solute/solvent interaction was calculated by MD simulations by putting a single solute molecule into a solvent box of fixed size.<sup>14</sup> The total theoretical curve is a sum of these three components, as shown in Figure 3A, for example, for the data at 100 ps. The fit between the experimental data and the theory was optimized by global fitting analysis<sup>14,15</sup> involving all  $q$  values and time delays in a single least-squares refinement. The multiplicative factors for the three components are not simple floating parameters but mathematically linked by energy and mass conservation and hydrodynamics.

Although the difference intensity  $q\Delta S(q)$  contains direct information on the structural changes, the real-space radial distribution functions (RDFs) provide a more intuitive picture of the structural dynamics. Obtained through sine-Fourier transforms of  $q\Delta S(q)$ , the RDF ( $r\Delta S(r)$ ) represents the experimental atom–atom pair distribution function during the course of the reaction.<sup>12–16</sup> The RDF is a measure, biased by the X-ray form factor, of the change in radial electron density around an (average) excited atom as a function of the interatomic distance,  $r$ . Figure 2B shows the  $r\Delta S(r)$  curve obtained by sine-Fourier transforms of  $q\Delta S(q)$  in Figure 2A. The prominent negative peak around 3 Å throughout all time delays is due to the depletion of the  $\text{Br}\cdots\text{Br}$  internuclear distance as  $\text{CBr}_4$  dissociates into  $\text{CBr}_3$  and  $\text{Br}$ . In addition to this peak, many new positive and negative peaks progress with time, but peak assignments are complicated because the three components contribute. Clear-cut assignment can be provided by decomposing these components as is done in the following section and in the section Structural Reaction Dynamics.

#### Solute-Only Diffraction Signal and Structural Dynamics.

In the global fitting analysis, the diffraction data are decomposed into the change due to the solute only, the change in the solvation cage, and the hydrodynamics response of the solvent. Figure 3 shows such decomposition for the data at 100 ps. From Figure 3B, it becomes clear that the positive peak around 4 Å and the negative peak around 7 Å come from the solute–solvent

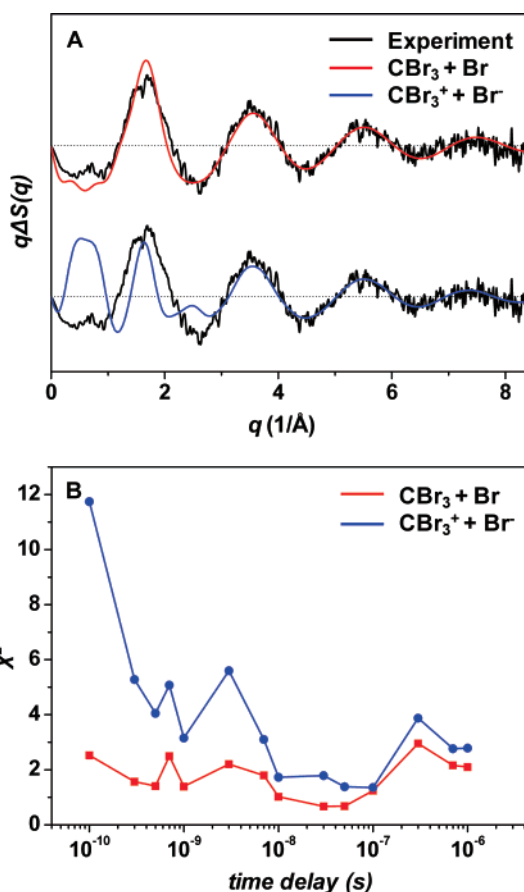


**Figure 7.** Comparison of the neutral channel ( $\text{CBr}_4 \rightarrow \text{CBr}_3 + \text{Br}$ ) and the ionic channel ( $\text{CBr}_4 \rightarrow \text{CBr}_3^+ + \text{Br}^-$ ). (A) Experimental data at 100 ps (in black) and the global fit results with the neutral channel (in red) and the ionic channel (in blue). (B) The  $\chi^2$  values as a function of time delays for the neutral channel (red rectangles) and ionic channel (blue circles). It is clear that the neutral channel fits our experimental data much better than that of the ionic channel. If both channels are included in the fit, the contribution of the ionic channel converges to zero.

cross term (cage term). In the same manner, the three components were decomposed for all time delays. Figure 4 shows  $q\Delta S(q)$  and  $r\Delta S(r)$  of the solute-only component, and Figure 5 shows  $r\Delta S(r)$  of the cage and solvent-only terms.

The solute-only term among the three components provides the most useful and direct information about the molecular structure of the reaction intermediates and reaction mechanism. To extract the solute-only dynamics from the experimental data, the bulk solvent response and the solvation cage structure of the theoretical model were subtracted from the measured total diffraction signals and compared to the difference Debye scattering intensities (Figure 4A). The agreement between the solute-only experimental data and the difference Debye scattering is very good, especially in the high  $q$  region  $q > 2.5 \text{ \AA}^{-1}$ . Due to the finite box size and approximate force field in molecular dynamics simulations, the cage structures calculated from MD influences the accuracy of the theoretical model.<sup>37</sup> Figure 4B shows the  $r\Delta S(r)$  curve obtained by sine-Fourier transforms of the  $q$ -curve in Figure 4A. The negative peak at 3.15 Å corresponds to the nonbonded  $\text{Br}\cdots\text{Br}$  distance in  $\text{CBr}_4$ . To minimize the contamination from the residual cage structure which could bias the interpretation of the structural dynamics of the solute only, the experimental data (Figure 4A) at  $q < 2.5 \text{ \AA}^{-1}$  was replaced by the theoretical difference Debye

(37) Cammarata, M.; Lorenc, M.; Kim, T. K.; Lee, J. H.; Kong, Q. Y.; Pontecorvo, E.; Lo Russo, M.; Schiro, G.; Cupane, A.; Wulff, M.; Ihee, H. *J. Chem. Phys.* **2006**, *124*, 124504.

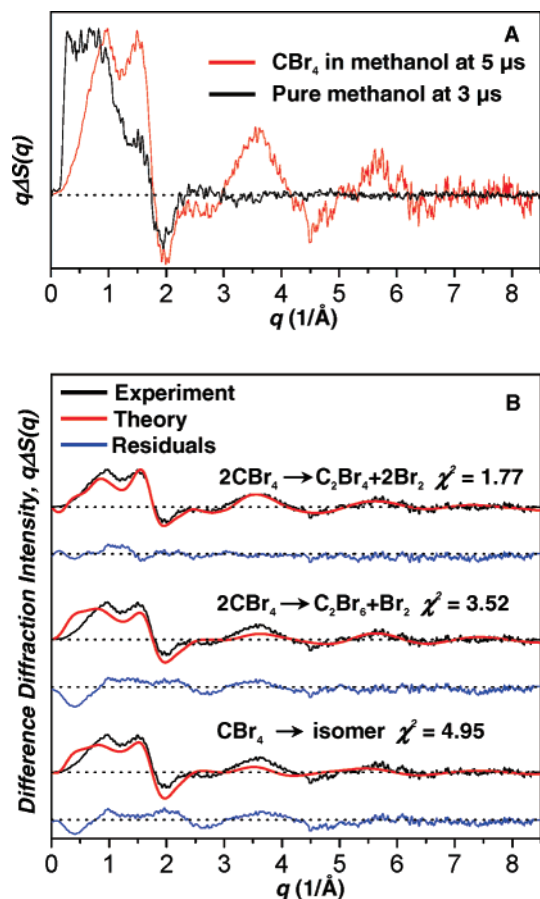


**Figure 8.** (A) Difference intensity of  $\text{CBr}_4$  in methanol at  $5 \mu\text{s}$ , and comparison with pure methanol at  $3 \mu\text{s}$  excited with an NIR (1500 nm) laser pulse. The strong diffraction signal at high  $q$  indicates that irreversible photoproducts are formed. (B) Determination of the photoproducts at  $5 \mu\text{s}$ . Experimental (black) and theoretical (red) difference diffraction intensities  $q\Delta S(q)$  for various candidate reaction channels and residues (blue) between experimental and theoretical curves are shown. The figure of merit  $\chi^2$  for different candidates indicates that  $\text{C}_2\text{Br}_4$  and  $\text{Br}_2$  are formed at longer time delays.

scattering intensities in the sine-Fourier transform. A similar approach is applied in electron diffraction to mask the effect from the beam-stop hole at low  $q$ .<sup>38,39</sup>

**Reaction Pathways of  $\text{CBr}_4$  in Methanol Determined from Global Fitting Analysis.** The global fitting analysis also yields the rate coefficients for a reaction model where all reasonable candidate reaction pathways were included (Supporting Information, Figure S1). The results are summarized in Figure 6, and details can be found in the Supporting Information.  $\text{CBr}_3$  and Br concentrations are dominant at early time, indicating the rupture of the C–Br bond in  $\text{CBr}_4$  by the UV optical excitation.<sup>28,35,40</sup> The Br radical decays rapidly into  $\text{Br}_2$  by nongeminate recombination with a rate constant of  $1.3 (\pm 4.5) \times 10^{10} \text{ M}^{-1} \text{ s}^{-1}$  which is similar to that in the neutral solvent  $\text{CCl}_4$  ( $1.5 \times 10^{10} \text{ M}^{-1} \text{ s}^{-1}$ ).<sup>41–43</sup> Most of  $\text{CBr}_3$  decays through

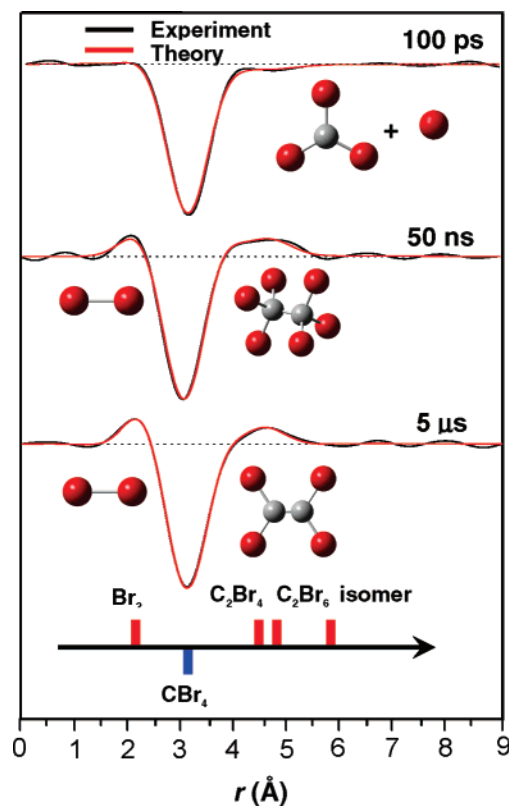


**Figure 9.** Change in the atom–atom pair distribution  $r\Delta S(r)$  for time delays at 100 ps, 50 ns, and  $5 \mu\text{s}$ . The blue bar indicates the nonbonded  $\text{Br}\cdots\text{Br}$  distance in  $\text{CBr}_4$ , while the red bars show the  $\text{Br}-\text{Br}$  bond length or nonbonded  $\text{Br}\cdots\text{Br}$  distances of the new molecules formed in the photodissociation reaction:  $\text{Br}_2$ ,  $\text{C}_2\text{Br}_4$ ,  $\text{C}_2\text{Br}_6$ , and the  $\text{Br}_2\text{CBr}-\text{Br}$  isomer. The molecular models for the major species at each time delay are also shown.

bimolecular recombination, which is typical of a nongeminate recombination reaction.<sup>44</sup> The main reaction of  $\text{CBr}_3$  is to escape from the solvation cage and to be trapped with another equivalent of  $\text{CBr}_3$  to give  $\text{C}_2\text{Br}_6$  with a rate constant of  $1.1 (\pm 2.5) \times 10^9 \text{ M}^{-1} \text{ s}^{-1}$ , which is an order of magnitude smaller than that of the recombination of  $\text{Br}_2$  from two Br radicals. This can be rationalized by the fact that compared to Br with an atomic radius of  $1.15 \text{ \AA}$ ,<sup>45</sup> the  $\text{CBr}_3$  radical has a larger molecular radius of around  $3.23 \text{ \AA}$ , which hinders its escape from the solvation cage and, thus, delays the nongeminate recombination reaction.

Since Br escapes from the solvation cage more readily and recombines to bromine in 10 ns while  $\text{CBr}_3$  stays in the cage for hundreds of nanoseconds, one may expect that  $\text{CBr}_3$  could undergo a further secondary C–Br bond breakage to give  $\text{CBr}_2$  and Br as observed in the gas-phase electron diffraction.<sup>46</sup>  $\text{CBr}_2$  is, however, not observed in the present experiment. This result is consistent with previous optical spectroscopic studies<sup>28,40</sup> where no  $\text{CBr}_2$  was detected in the liquid-phase photodissociation of carbon tetrabromide excited with the same laser photons at 266 nm. Our DFT calculations with a solvent model<sup>35</sup> showed that 2.7 eV is needed to dissociate  $\text{CBr}_3$  whereas the maximum access energy is only 2.2 eV. Thus, the formation of  $\text{CBr}_2$  can be excluded.

(38) Ihee, H.; Lobastov, V. A.; Gomez, U. M.; Goodson, B. M.; Srinivasan, R.; Ruan, C. Y.; Zewail, A. H. *Science* **2001**, *291*, 458.

(39) Ihee, H.; Goodson, B. M.; Srinivasan, R.; Lobastov, V. A.; Zewail, A. H. *J. Phys. Chem. A* **2002**, *106*, 4087.

(40) (a) Zheng, X. M.; Kwok, W. M.; Phillips, D. L. *J. Phys. Chem. A* **2000**, *104*, 10464. (b) Zheng, X. M.; Phillips, D. L. *J. Phys. Chem. A* **2000**, *104*, 6880. (c) Zheng, X. M.; Phillips, D. L. *Chem. Phys. Lett.* **2000**, *324*, 175.

(41) Abul-Haj, N. A.; Kelley, D. F. *Chem. Phys. Lett.* **1985**, *119*, 182.

(42) Zhu, X. R.; Harris, J. M. *Chem. Phys. Lett.* **1991**, *186*, 183.

(43) Zhu, X. R.; Harris, J. M. *J. Phys. Chem.* **1993**, *97*, 6650.

(44) Wulff, M.; Bratos, S.; Plech, A.; Vuilleumier, R.; Mirloup, F.; Lorenc, M.; Kong, Q. Y.; Ihee, H. *J. Chem. Phys.* **2006**, *124*, 034501.

(45) Slater, J. C. *J. Chem. Phys.* **1964**, *41*, 3199.

(46) Ivey, R. C.; Schulze, P. D.; Leggett, T. L.; Kohl, D. A. *J. Chem. Phys.* **1974**, *60*, 3174.

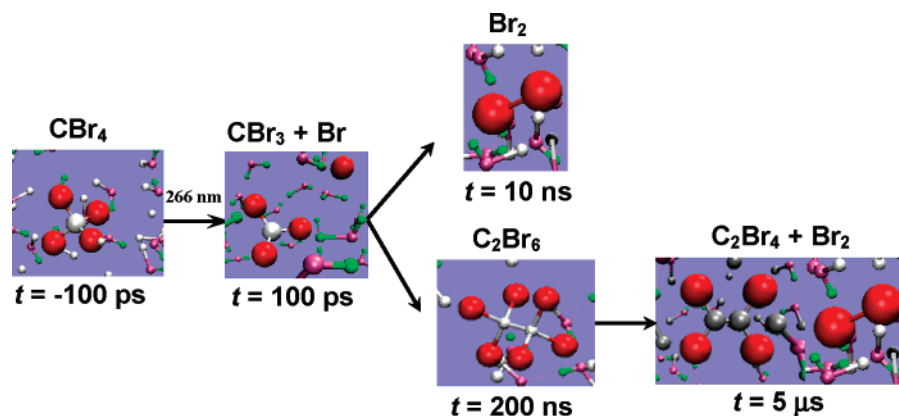


**Figure 10.** A schematic photochemical reaction mechanism of  $\text{CBr}_4$  in methanol determined by time-resolved X-ray diffraction in solution.

Our DFT study<sup>35</sup> shows that the bimolecular recombination reaction of  $\text{CBr}_3$  is exothermic and  $\text{C}_2\text{Br}_6$  can be formed directly without an energy barrier. However, the concentration of  $\text{C}_2\text{Br}_6$  does not increase accordingly as  $\text{CBr}_3$  decays with time (Figure 6), which indicates that  $\text{C}_2\text{Br}_6$  is not stable and dissociates quickly. Eventually,  $\text{C}_2\text{Br}_6$  decays to  $\text{Br}_2$  and a new species,  $\text{C}_2\text{Br}_4$ , as the final products in microseconds, with a rate constant of  $5.8 (\pm 6.5) \times 10^6 \text{ s}^{-1}$ . At longer time delays, the stable bromine and  $\text{C}_2\text{Br}_4$  molecules become the dominant solute species. Careful inspection of Figure 6 reveals that  $\text{Br}_2$  has already formed at 100 ps and the different concentrations between  $\text{Br}$  and  $\text{CBr}_3$  at 100 ps indicates that  $\text{Br}_2$  is formed through nongeminate recombination of  $\text{Br}$ . At late time delays,  $\text{Br}_2$  is formed from  $\text{C}_2\text{Br}_6$  dissociation.

We also considered the possibility of electron-transfer processes. Although the energy (7.87 eV) required to generate  $\text{CBr}_3^+$  and  $\text{Br}^-$  from  $\text{CBr}_4$  is much larger than the photon energy (4.66 eV), it was suggested that the solvation energy may be large enough to overcome the energy deficiency.<sup>29</sup> Since the molecular structure and the relative energy level of  $\text{CBr}_3^+$  are different from those of  $\text{CBr}_3$ , time-resolved diffraction should be able to distinguish those two channels. We checked this point by comparing the global fit results of those two channels as shown in Figure 7. The  $\chi^2$  values of the fit using the ionic channel model are significantly larger than those using the neutral channel model as shown in Figure 7B. Figure 7A shows a comparison of global fitting results using the two models for the data at 100 ps as an example. More importantly, if we include both channels in the fit, the contribution of the ionic channel vanishes. Thus it is clear that the neutral channel fits our experimental data much better than that of the ionic channel. It is interesting to observe that the differentiation between the two models mostly comes from the low  $q$  region where the contribution from the solute–solvent cross term and the solvent-only term is relatively large compared with that for the high  $q$  region.

In a previous time-resolved absorption spectroscopic study of the photolysis of  $\text{CBr}_4$  at 266 nm, various nonpolar and polar solvents such as cyclohexane, dodecane, 1-octanol, 2-propanol, acetonitrile, and propylene carbonate were used, and their results showed that the decay time constants of their transient clearly depend on the polarity of solvent and range from subnanoseconds to microseconds.<sup>29</sup> Among their solvents, acetonitrile has a dielectric constant of about 37 which is very close to methanol's dielectric constant of about 33. They

attributed the observed transients to the solvated ion pair  $(\text{CBr}_3^+//\text{Br}^-)_{\text{solv}}$  with a decay time constant of about 4 ns. In our experiment in methanol, within 4 ns, we observe only  $\text{CBr}_3$ ,  $\text{Br}$ , and  $\text{Br}_2$ . On the other hand, in a transient resonance Raman study, the same transient corresponding to the solvated ion pair was assigned to the  $\text{Br}_2\text{CBr}-\text{Br}$  isomer in cyclohexane.<sup>28</sup> We considered the possibility of forming this isomer via geminate recombination of  $\text{CBr}_3$  and  $\text{Br}$  by including the isomer formation channel in the fit. However, the global fitting results show that its formation is negligible. Our results suggest that the isomer or the solvated ion pair observed in previous time-resolved spectroscopic studies could not be detected within the signal-to-noise ratio of the current data and their formation should be a minor channel compared with those observed clearly by time-resolved diffraction.

**Elucidation of Final Reaction Products.** In contrast to our previous observation in the reversible photodissociation of iodine in  $\text{CCl}_4$ ,<sup>12</sup> where the solute dynamics is finished in a few tens of nanoseconds and the bulk solvent dominates the signal at late time delay, strong solute signals are still observed at 1  $\mu\text{s}$  in the present study. To follow the kinetics of forming final products, experimental data at 5  $\mu\text{s}$  were also collected. Since the liquid flows at a speed of 3 m/s and the X-ray beam size is 60  $\mu\text{m}$ , it takes 20  $\mu\text{s}$  for the X-ray probed liquid to move out. At 5  $\mu\text{s}$ , the longest delay considered in this study, 75% of the laser excited liquid is still in the X-ray beam and 25% of new liquid moves in. Considering the larger laser spot size of  $180 \times 150 \mu\text{m}$  (fwhm, horizontal  $\times$  vertical) and the flow speed of the liquid, a Gaussian integral of the laser intensity in the X-ray slit shows that it is 2.5% smaller after 5  $\mu\text{s}$  due to the moving sample. The perturbation of the new liquid can thus be neglected. The experimental data at 5  $\mu\text{s}$  still probes the continuous dynamics of the photoproducts.

As a control experiment, pure methanol was excited with near-infrared (NIR) optical photons at 1500 nm,<sup>37</sup> and the difference signal at 3  $\mu\text{s}$  is shown together with the signal from  $\text{CBr}_4$ /methanol at 5  $\mu\text{s}$  in Figure 8A. Whereas the signal from pure methanol is flat at high  $q$ , strong oscillations are observed for the photodissociation of carbon tetrabromide at 5  $\mu\text{s}$ , indicating that irreversible photoproducts are formed. To determine the final photoproducts on the microsecond time scale, the measured difference diffraction intensity  $q\Delta S(q)$  at 5  $\mu\text{s}$  was fitted to a series of candidate molecules (Figure 8B). The fit for the reaction channel  $\text{CBr}_4 \rightarrow \frac{1}{2}\text{C}_2\text{Br}_4 + \text{Br}_2$  almost perfectly matches the experimental data over the whole  $q$  range while

the reaction channels for  $\text{C}_2\text{Br}_6$  and isomer yield poor agreement with the experiment. The residuals between the experiment and the fits (blue curves in Figure 8B) as well as the figure of merit ( $\chi^2$ ) confirm that the  $\text{Br}_2 + \text{C}_2\text{Br}_4$  model fits the data better than the other models. It is worth noting that when all possible solutes,  $\text{CBr}_3$ ,  $\text{Br}$ ,  $\text{Br}_2\text{CBr}-\text{Br}$  isomer,  $\text{CBr}_2$ ,  $\text{C}_2\text{Br}_6$ ,  $\text{C}_2\text{Br}_5$ ,  $\text{C}_2\text{Br}_4$ , and  $\text{Br}_2$ , are included simultaneously in the fit at  $5 \mu\text{s}$ , only  $\text{C}_2\text{Br}_4$  and  $\text{Br}_2$  remain after the least-square refinement, and the others converge to zero. We further confirmed the final reaction products by UV/vis spectroscopy and NMR measurements before and after photolysis (Supporting Information). The first confirmed the existence of  $\text{Br}_2$  by its characteristic absorption band, and the latter showed that the only carbon-containing photoproduct has double bond character, thus providing evidence for  $\text{C}_2\text{Br}_4$ .

**Structural Reaction Dynamics.** The radial distribution function (RDF)  $r\Delta S(r)$  gives a more intuitive picture of the structural dynamics of putative solutes as they provide the distribution of atomic pairs  $\text{Br}-\text{Br}$  and  $\text{C}-\text{Br}$  in the solute molecule as a function of time. Figure 9 shows the experimental and theoretical functions  $r\Delta S(r)$  at 100 ps, 50 ns, and  $5 \mu\text{s}$ . The strong negative peak at  $3.15 \text{ \AA}$  starting at 100 ps indicates the  $\text{C}-\text{Br}$  bond ruptures in the parent molecule,  $\text{CBr}_4$ . Since  $\text{CBr}_4$  has a tetragonal symmetry, there are six  $\text{Br}\cdots\text{Br}$  and four  $\text{C}\cdots\text{Br}$  nearest neighbor pairs; in  $\text{CBr}_3$  these pairs reduce to three for both  $\text{Br}\cdots\text{Br}$  and  $\text{C}\cdots\text{Br}$ . The Debye scattering intensity is weighted by  $Z_i \times Z_j / r_{ij}$ , where  $Z_i$  and  $Z_j$  are the atomic numbers, and  $r_{ij}$ , the distance between atoms. With  $r_{\text{Br}\cdots\text{Br}} = \sqrt{8/3} \times r_{\text{C}\cdots\text{Br}}$ ,  $Z_{\text{Br}} = 35$ , and  $Z_{\text{C}} = 6$ , the scattering intensity from  $\text{Br}\cdots\text{Br}$  change is 10.7 times stronger than that for  $\text{C}-\text{Br}$  change. The  $r\Delta S(r)$  signals are thus dominated by the  $\text{Br}\cdots\text{Br}$  correlation. The minimum at  $3.15 \text{ \AA}$  persists beyond  $5 \mu\text{s}$ , indicating that the photodissociation reaction of  $\text{CBr}_4$  is irreversible. New features appear as time progresses, indicating that new species must be formed.  $\text{C}_2\text{Br}_6$  has different nonbonded  $\text{Br}\cdots\text{Br}$  distances ranging from  $3.20$  to  $4.74 \text{ \AA}$ <sup>35</sup> and ought to have a strong diffraction signature due to the large scattering power of bromine. The broad peak at  $4.75 \text{ \AA}$  appearing at 50 ns is an overlap of diffraction from different  $\text{Br}\cdots\text{Br}$  correlations, and it is attributed to the nonbonded  $\text{Br}\cdots\text{Br}$  distances in  $\text{C}_2\text{Br}_6$  as shown in Figure 9. Two clear maxima at  $2.25$  and  $4.65 \text{ \AA}$  appear at  $5 \mu\text{s}$ , indicating the presence of  $\text{Br}_2$  and  $\text{C}_2\text{Br}_4$  at late time delay. The  $4.65 \text{ \AA}$  peak is assigned to the diagonal  $\text{Br}\cdots\text{Br}$  distance in  $\text{C}_2\text{Br}_4$  as shown in Figure 9.

Based on the structural dynamics of various solutes as a function of time, a photodissociation mechanism of tetrabromomethane in methanol is proposed: the  $\text{C}-\text{Br}$  bond rupture in  $\text{CBr}_4$  leads to  $\text{CBr}_3$  and  $\text{Br}$ . The radicals escape from the solvent cage and recombine nongeminately, giving  $\text{Br}_2$  and  $\text{C}_2\text{Br}_6$ . Further,  $\text{C}_2\text{Br}_6$  eventually decays into  $\text{C}_2\text{Br}_4$  and  $\text{Br}_2$  as the final products. A schematic photodissociation reaction mechanism is shown in Figure 10.

## Conclusions

Time-resolved X-ray diffraction reveals the following complicated photodissociation reaction pathways of tetrabromomethane in methanol over a wide temporal range from 100 ps to  $5 \mu\text{s}$ . Upon excitation, a  $\text{C}-\text{Br}$  bond in the parent  $\text{CBr}_4$  molecule is cleaved to yield the  $\text{CBr}_3$  and  $\text{Br}$  radicals. Then,  $\text{CBr}_3$  and  $\text{Br}$  escape from the solvent cage and combine nongeminately to form  $\text{C}_2\text{Br}_6$  and  $\text{Br}_2$ , respectively. The  $\text{Br}_2\text{CBr}-\text{Br}$  isomer formed by geminate recombination or the solvated ion pair observed in previous time-resolved spectroscopic studies could not be detected within the current signal-to-noise ratio, and this suggests that their formation should be a minor channel compared with those observed in this work.  $\text{C}_2\text{Br}_6$  eventually decays to  $\text{C}_2\text{Br}_4$  and  $\text{Br}_2$  as the final stable products. X-ray diffraction offers an important advantage that the scattered X-rays contain contributions from all chemical species simultaneously and the diffraction signal from each chemical species can be quantitatively calculated from molecular structures and compared with experimental data. For this reason, the geometries of various short-lived intermediates, and stable products alike ( $\text{CBr}_3$ ,  $\text{Br}$ ,  $\text{C}_2\text{Br}_6$ ,  $\text{C}_2\text{Br}_4$ , and  $\text{Br}_2$ ), and the associated rate constants connecting complex reaction pathways could be determined with an  $\sim 0.01 \text{ \AA}$  spatial resolution and  $\sim 100$  ps time resolution with the aid of global fitting analysis involving diffraction signals at all time delays.

**Acknowledgment.** The authors would like to thank Marco Cammarata, Manuela LoRusso, Friederike Ewald, and Tae Kyu Kim for their help in the experimental setup and data collection; Michel H. J. Koch for valuable discussion and help; and Kwang Hoon Jun, Jong Hyeok Lee, Kyung Hwan Kim, Jangbae Kim, and Jungkweon Choi for their help in the final photoproduct analysis using UV/vis and NMR spectroscopy. This work was supported by the EU Grants FAMTO (HPRICT-1999-50004) and FLASH (FP6-503641) and by Creative Research Initiatives (Center for Time-Resolved Diffraction) of MOST/KOSEF awarded to H.I.

**Supporting Information Available:** Kinetics of the photodissociation of  $\text{CBr}_4$ ; Hydrodynamics of the bulk solvent; Geometry of  $\text{CBr}_3$  and  $\text{CBr}_3^+$  in methanol calculated at B3LYP/6-311+G(3df) level; Geometries and bond lengths of various molecules  $\text{CBr}_4$ ,  $\text{CBr}_3$ ,  $\text{CBr}_2$ ,  $\text{Br}_2$ ,  $\text{C}_2\text{Br}_6$ ,  $\text{C}_2\text{Br}_4$ ,  $\text{CBr}_3-\text{Br}$  isomer,  $\text{CBr}_3^+$ , and  $\text{C}_2\text{Br}_5$  in methanol calculated at B3LYP/6-311+G(3df) level; UV/vis and NMR spectra before and after photolysis; UV/vis spectra of  $\text{CBr}_4$  at various concentrations; and Complete citation of ref 31. This material is available free of charge via the Internet at <http://pubs.acs.org>.

JA073503E